

Numerical scheme for non-linear model of supercritical fluid extraction from polydisperse ground plant material: single transport system

A Salamatın

Kazan Federal University, Department of Aerohydromechanics, Kremlyovskaya str.,
 18, Kazan 420008, Russia

E-mail: arthur.salamatın2@gmail.com

Abstract. Numerical algorithm is developed for modelling non-linear mass transfer process in supercritical fluid extraction (SFE). The ground raw material is considered as polydisperse, characterized by discrete number of effective particle fractions. Two continuous interacting counterparts separated by permeable membrane are distinguished in plant material build-up. The apoplast plays role of transport channels during extraction, and symplast contains extractable oil. The complete SFE model is non-linear as a result of non-linearity of oil dissolution kinetics. The computational scheme is based on the finite-volume approximation method and Thomas elimination procedure. The resulting system of algebraic equations is solved iteratively. Special attention is paid to polydisperse substrates, when particle scale characteristics of all fractions interact with each other through pore phase concentration on the vessel scale. Stability of the developed algorithm is demonstrated in numerical tests. Special iterative procedure guarantees a monotonic decrease of oil content in individual particles of substrate. It is also shown that in the limit of the so-called shrinking core approach the number of mesh nodes on a particle scale should be increased.

1. Problem formulation

Supercritical Fluid Extraction (SFE) – is a technological approach to extract natural compounds from particles of ground plant material. Conventionally, the complete model of the process consists of two submodels [1], external and internal. The first accounts for convective solvent flow through a porous media, composed of polydisperse ground plant material particles. After [1, 2], external mass balance is described in one-dimensional quasi-stationary approximation, and master-equation takes the following form

$$\frac{\partial c}{\partial \zeta} = \sum_{i=1}^n \frac{Sh_i}{a_i^2} (\theta_{b,i} - c) f_i, \quad c|_{\zeta=0} = 0. \quad (1)$$

Here, $0 \leq c \leq 1$ is the solute concentration in the pore phase, ζ – axial coordinate along the vessel, varying from zero at the inlet to normalized vessel height H at the outlet, f_i and Sh_i are volume fraction and Sherwood number, corresponding to i -th fraction of plant material, a_i – dimensionless radius of spherical particle, $1 \leq i \leq n$. Solute concentration θ_b at the particle surface is determined from the solute flux continuity condition (4). All Sherwood numbers Sh_i are assumed to be tending to infinity.

The internal submodel is of particular importance for correct SFE modeling and understanding. The one considered here contains two similarity criteria, Θ and M . The relative solvent dissolution capacity



Θ characterizes the raw material. The second criterion, $M \sim a^2$, distinguishes particle fraction (of size a) and varies from zero to infinity, what corresponds to various internal extraction regimes. The case of vegetable and fatty oil extraction is considered in this work. So, the solvent dissolution capacity $\Theta \rightarrow 0$.

The detailed description of plant material structure leads to two mass balance equations

$$\frac{\partial x_s}{\partial \tau} + (1 + M)(\theta_s - \theta_a) = 0, \quad (2)$$

$$6M(\theta_s - \theta_a) + \Delta \theta_a = 0, \quad (3)$$

with boundary conditions

$$\frac{\partial \theta_a}{\partial r} \Big|_{r=0} = 0, \quad \theta_a \Big|_{r=1} = \theta_b, \quad -\frac{\partial \theta_a}{\partial r} \Big|_{r=1} = \text{Sh}(\theta_b - c) \quad (4)$$

for normalized solute concentration $0 \leq \theta_a \leq 1$ within transport channels, and initial condition

$$x_s \Big|_{t=0} = 1 \quad (5)$$

for normalized oil density $0 \leq x_s \leq 1$ which accounts for extractable oil inclusions, as well as dissolved solute inside cells. Here, $0 \leq r \leq 1$ is the normalized radial coordinate inside spherical particles, and τ – dimensionless extraction time related to a particular particle fraction

$$\tau_i = \frac{1 + M_i}{1 + M_1} \tau_1 \equiv A_i \tau_1.$$

Common SFE process time t is associated with the first fraction, $t = \tau_1$.

The normalized intra-cell solute concentration $0 \leq \theta_s \leq 1$ depends on x_s , and is determined by the process of oil inclusions dissolution in the solvent. The dissolution model considered here leads to the following non-linear expression

$$\theta_s = \min\{1, x_s / \Theta\}. \quad (6)$$

The internal submodel, Eqs. (2)-(6), should be solved for every i -th particle fraction. All characteristics are attributed to a particular particle fraction i , the index is omitted where there is no ambiguity.

The moving boundary $r = R$ appears inside each individual particle and is controlled by the assumed dissolution model (6) at relatively low solvent dissolution capacity, $\Theta < 1$. The boundary separates internal core with drop-phase oil, $x_s > \Theta$, from outer transport zone where all oil is completely dissolved in the solvent, $x_s < \Theta$. Position of this boundary is unknown *a priori* and must be determined in the course of modeling. Obviously, at the beginning of the process $R(a, \zeta, 0) \equiv 1$, since no solute is extracted from substrate.

Eqs. (1)-(6), formulated above, form a complete simplified model of the SFE process. They consider intra-particle solute diffusion in quasi-stationary approximation and account only for one transport system. Nevertheless, these equations reveal the principal peculiarities and problems encountered in numerical SFE modeling.

2. Numerical algorithm

Let us introduce uniform spatial meshes $\zeta_j = h_\zeta j$, $h_\zeta = H / m_\zeta$, $j = 0, 1 \dots m_\zeta$ and $r_l = h_r l$, $h_r = 1 / m_r$, $l = 0, 1 \dots m_r$ in the extractor column and particles respectively. Unknown discrete analogues c_{jk} , $x_{s,ijk}$, $\theta_{a,ijk}$, $\theta_{s,ijk}$, and $\theta_{b,ijk}$ of process characteristics, c , x_s , θ_a , θ_s , and θ_b , are calculated successively at time moments $t_k = h_t k$, $k = 1, 2 \dots$ according to the following algorithm. The subscripts j, l, k as well as i are omitted further if there is no ambiguity.

The following finite-difference scheme is deduced on the basis of well-developed integral interpolation (or finite volume) method [3, 4]

$$\frac{c_j - c_{j-1}}{h_\zeta} = \sum_{i=1}^n \frac{\text{Sh}_i}{a_i^2} (\theta_{b,ij} - c_j) f_i, \quad c_0 = 0, \quad (7)$$

$$\frac{x_s - \tilde{x}_s}{Ah_t} + (1 + M)(\theta_s - \theta_a) = 0, \quad (8)$$

$$2M(r_{l+1/2}^3 - r_{l-1/2}^3)(\theta_{s,l} - \theta_{a,l}) + r_{l+1/2}^2 \frac{\theta_{a,l+1} - \theta_{a,l}}{h_r} - r_{l-1/2}^2 \frac{\theta_{a,l} - \theta_{a,l-1}}{h_r} = 0, \quad (9)$$

$$Mh_r(\theta_{s,0} - \theta_{a,0}) + \frac{\theta_{a,1} - \theta_{a,0}}{h_r} = 0, \quad (10)$$

$$2M(1 - r_{m_r-1/2}^3)(\theta_{s,m_r} - \theta_{a,m_r}) - \text{Sh}(\theta_{a,m_r} - c) - r_{m_r-1/2}^2 \frac{\theta_{a,m_r} - \theta_{a,m_r-1}}{h_r} = 0. \quad (11)$$

Here, vector $\tilde{x}_s = x_{s,k-1}$ is known from previous $(k-1)$ -th time layer, and algebraic expression (6) remains unchanged.

The computational scheme is based on Thomas elimination procedure [5]. First, the sweep run through Eqs. (8)-(11), and (6) delivers coefficients α and β for the linear relation between θ_b and c

$$\theta_b = \alpha c + \beta.$$

Next, c is found after substitution of the latter expression into Eq. (7). It allows to perform the second step of Thomas procedure – backward substitution, and complete the calculation of the solute characteristics from the internal model. According to Eq. (7), these parameters are sequentially determined for every cross-section ζ_j along the fluid flow. Internal submodel could be solved separately for every particle size only at ζ_0 , where $c_0 = 0$ is fixed.

The coefficients α and β are found after linearization of Eq. (6), and Thomas algorithm is then applied to solve the internal-model equations. As it is already mentioned, there is a moving boundary R in every particle, that separates the internal oil saturated core and outer transport zone. The minimum of the right-hand side of Eq. (6) is well defined in every zone, and complete internal submodel is linear for $r < R$ and $r > R$. Current discrete boundary position R_k is ascribed to mesh points r_l , and it is determined iteratively for every particle fraction. The initial guess is $R^{(1)} = R_{k-1}$, since R monotonically decreases with time, and

$$\theta_s = \begin{cases} 1, & \text{if } r \leq R^{(1)}; \\ x_s / \Theta, & \text{if } r > R^{(1)}. \end{cases} \quad (12)$$

The corresponding vectors $x_s^{(1)}$, and $\theta_s^{(1)}$, as well as $R^{(1)}$ have to be checked for consistency with relation (12) in the neighbourhood of $r = R^{(1)}$. For any set I of particle fractions which are inconsistent with the above conditions the guess for R should be decreased, $R_l^{(2)} = R_l^{(1)} - h_r$. Boundary positions in other fractions, $i \notin I$, are not modified. With the new guess $R^{(2)}$ another iteration is executed. The iterative procedure is continued till Eq. (6) is satisfied for every particle fraction i , i.e. the set I turns out empty. Then, unknown values could be determined at the next vessel cross-section, ζ_{j+1} , according to the same procedure.

Eventually, the solution of simultaneous algebraic Eqs. (6)-(11) could be found after a finite number of iterations for any polydisperse packed bed, since the core radius $0 \leq R \leq 1$, and it monotonically decreases in the course of extraction.

3. Single particle washed by pure solvent

Let us consider a single particle washed by pure solvent, at $c = 0$. Under this assumption internal submodel (8)-(11), and (6) can be solved independently to study the convergence of the computational algorithm.

Various extraction regimes take place on the particle scale during extraction, as predicted by the model, Fig. 1. At small Θ , they are primarily determined by M . As one can see, a boundary layer develops in the neighborhood of $r = R$, and its thickness decreases with $M \rightarrow \infty$. Thus, it could not be adequately resolved by the mesh at constant m_r . A noticeable concentration c deviation from the exact value can occur if this fact is disregarded, as demonstrated in the next section. Still, the scheme

remains stable, and integral extraction process characteristic, Overall Extraction Curve (OEC) [1, 2, 6-9], is insensitive to this deviation.

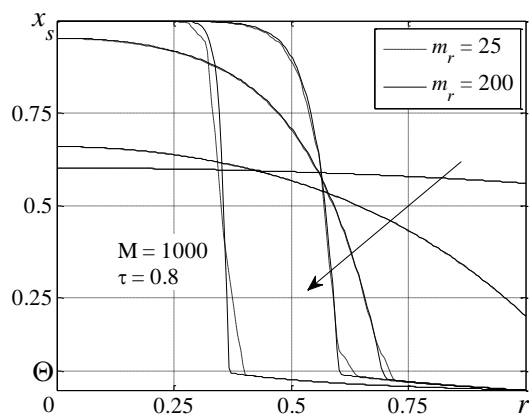


Figure 1. $x_s(r)$ at different M ; $\Theta = 0.05$. Arrow indicates $\lg M$ increase from -1 to 2 at step 1, and lines are obtained at $\tau = 0.5$. Label corresponds to the fifth pair of curves.

The limit of $M \rightarrow \infty$ is termed as the Shrinking Core (SC) pattern [2, 6, 7]. The model (6)-(11) at high values of M is of particular interest from the computational point of view, since x_s curve is not smooth and the jump develops in the neighborhood of $r = R$ at these conditions. The case of $M = 100$ and $\Theta = 0.05$ is analyzed in Figs. 2, and 3. The curves are plotted for $m_r = 25$ (dashed lines), and 200 (solid lines), and demonstrate convergence of the computational algorithm on the particle scale. Arrows indicate direction of time t increase from 0.2 to 0.8 at step 0.2, and solution does not depend on h_t when it is below 0.01. The scheme convergence is apparent, and a relatively small number $m_r \sim 100$ of mesh points is sufficient to obtain a reliable solution in this case.

4. Monodisperse packed beds

The scheme (6)-(11) convergence is studied in this section for monodisperse packed bed, at $n = 1$. This simple approximation is commonly used in the kinetics data interpretation [7-9]. It is important from the computational point of view that, unlike in polydisperse packed beds, the moving internal oil-core interfaces in different particles are locally identical, and internal moving boundaries R do not mutually affect each other. So, a unique problem (6)-(11) solution exists, and it could be found after a finite number of iterations.

It is found that vessel scale mesh at $m_\zeta \sim 100$ is well sufficient for a wide spectrum of process parameters, and it is independent of H -value, while time step h_t must be normally chosen on the order of 0.001. Special attention should be paid to the m_r impact onto external submodel solution. Inadequate spatial resolution of non-smooth distributions of internal characteristics, x_s , and θ_s on the particle scale at high M can noticeably affect the pore phase concentration c , as demonstrated in Fig. 4. Here, curves correspond to $H = 20$, $\Theta = 0.05$, and extreme value of $M = 1000$, and are calculated at a relatively small $m_r = 25$. However, the computational errors become negligible with increase in m_r , at $m_r = 200$, and vanish with time, and they practically do not affect OEC. Hence, the major computational inaccuracy develops when only a particle superficial layer is under extraction. The convergence of the solvent flow characteristics is demonstrated in Fig. 5 for the same values of process and scheme parameters. Thus, the required accuracy of the numerical solution is mainly controlled by the quality of computations on the particle scale with the c -errors inherited via Eq. (11).

5. Bidisperse packed beds

Here, the convergence of computational algorithm is studied in a particular case of polydisperse packs, bidisperse ground plant material, for $n = 2$. This model of packed beds is used for detailed interpretation of SFE kinetics data [2].

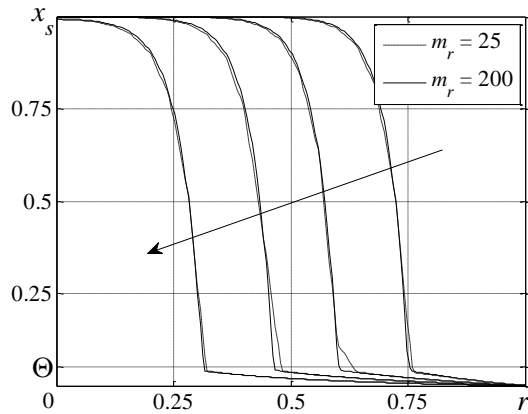


Figure 2. $x_s(r)$ dependence at different time moments t .

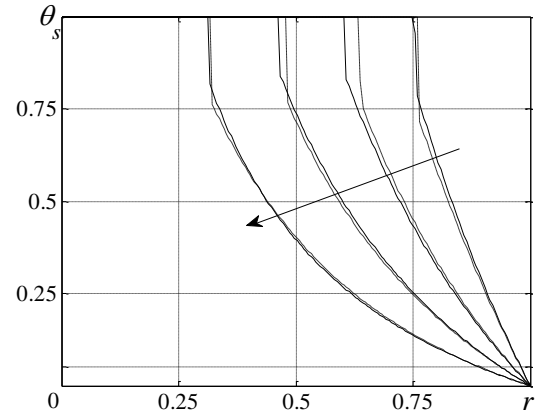


Figure 3. $\theta_s(r)$ dependence at different time moments t .

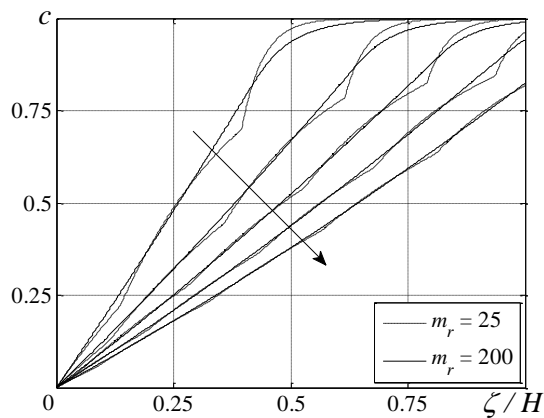


Figure 4. $c(\zeta)$ at different moments. Arrow indicate t increase from 0.02 to 0.1 at step 0.02.

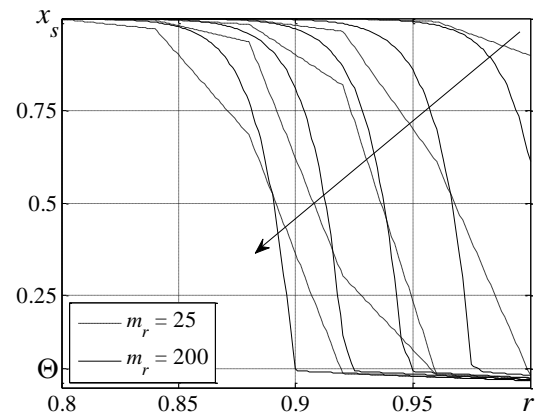


Figure 5. $x_s(r, \zeta = H / 2)$ at different moments. Arrow indicate t increase from 0.02 to 0.1 at step 0.02.

In bidisperse substrates (as well as polydisperse, at $n > 2$), moving oil-core boundaries R_i locally interact with each other through the pore phase concentration c , and should be calculated simultaneously for each fraction in every cross-section ζ . Physically consistent computational algorithm to solve the problem is described above in Sec. 2, and explicitly accounts that all R_{ij} do not increase in the course of extraction. It allows to determine a unique solution for a given set of SFE parameters and mesh characteristics.

Conventionally, bidisperse packed bed contains particles of two distinct size modes, $a_1 \ll a_2$, and it is set hereinafter that $M_1 = M_2 / 100$. This situation is typical for laboratory-scale experiments [2, 8, 9]. Accordingly, the substrate is characterized by two sets of spatial and time scales which manifest themselves in respective profiles of pore solute concentration versus ζ and t as illustrated by Figs. 6, and 7. Here, $\Theta = 0.05$, $M_2 = 100$, $f_1 = 0.2$, $H = 2000$, $m_\zeta = 200$, and 25 (for solid and dashed lines), $h_t = 0.03$. Arrow indicates t increase from 8 to 32 at step 8. The convergence on the particle scale is provided by $m_r = 200$.

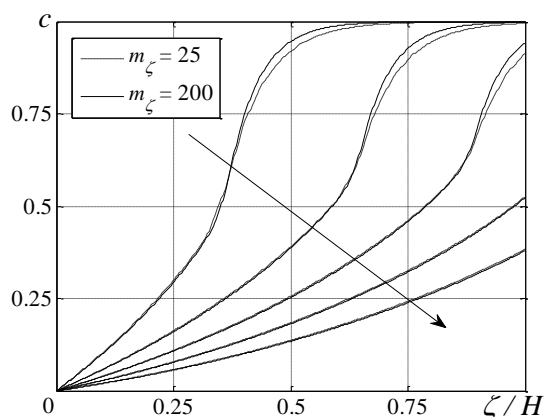


Figure 6. Pore phase concentration $c(\zeta)$ at different time moments. Bidisperse packed bed.

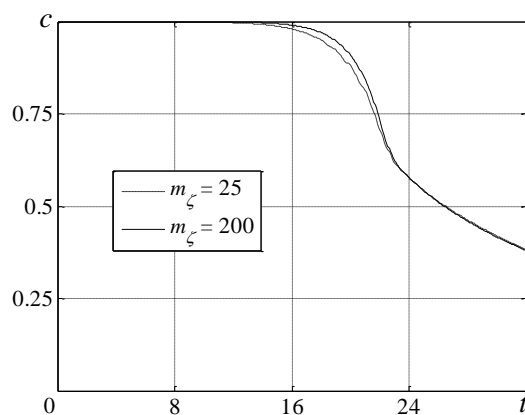


Figure 7. Outlet pore phase concentration $c(t, \zeta = H)$. Bidisperse packed bed.

6. Conclusion

The finite difference algorithm is developed to solve numerically the non-linear SFE model with the detailed description of ground plant material structure on the particle scale, and packed bed polydispersity on the vessel scale.

The scheme convergence is analyzed and demonstrated on both scales. Mesh characteristics m_ζ and h_i are specified to provide high accuracy of simulations in a wide range of process parameters. Yet, the universal estimates for the mesh detalization, m_r , on the particle scale do not exist, since the solution of the internal submodel is not smooth at $M \rightarrow \infty$. Nevertheless, the overall integral characteristic, OEC, remains rather stable. It is found that m_r could be varied up to 200 for M up to 100.

The developed iterative computational scheme is shown to be stable and provides realistic monotonous decrease of all R_{ij} during extraction, and, therefore, could be considered as physically consistent. Apparently, a scheme with better convergence characteristics could be developed if current R -value is explicitly accounted in the quadrature formula used in finite volume method. However, it leads to a substantial complication of numerical scheme.

Acknowledgments

This study was supported by the Russian Foundation for Basic Research and by the Academy of Science of Republic of Tatarstan through the grant No. 15-41-02542 r_povolzhe_a, and grant No. 16-31-00007 mol_a.

References

- [1] Egorov A G, Salamatina A A, and Maksudov R N 2014 *Theor. Found. Chem. Eng.* **48** 39
- [2] Egorov A G and Salamatina A A 2015 *Chem. Eng. Technol.* **38** 1203
- [3] Patankar S V 1980 *Numerical Heat Transfer and Fluid Flow* (New York: Hemisphere)
- [4] Samarskii A A 2001 *The Theory of Difference Schemes* (New York: Hemisphere)
- [5] Conte S D and deBoor C 1972 *Elementary Numerical Analysis* (New York: McGraw-Hill)
- [6] Salamatina A A and Egorov A G 2015 *J. Supercrit. Fluids* **105** 35
- [7] Goto M, Roy B C, and Hirose T 1996 *J. Supercrit. Fluids* **9** 128
- [8] Salgin U and Korkmaz H 2011 *J. Supercrit. Fluids* **58** 239
- [9] Ozkal S G, Yener M E and Bayindirli L. 2005 *J. Supercrit. Fluids* **35** 119